ELSEVIER

Journal of Alloys and Compounds 229 (1995) 206–215

Journal of ALLOYS AND COMPOUNDS

Quaternary chalcogenides containing a rare earth and an alkali- or alkaline-earth metal

Ping Wu, James A. Ibers*

Department of Chemistry, Northwestern University, Evanston, IL 60208-3113, USA

Received 12 December 1994

Abstract

This paper reviews the recent synthesis and characterization of quaternary solid-state compounds that contain three metal elements from different major blocks of the Periodic Table, namely an *s*-block alkali- or alkaline-earth metal, an *f*-block lanthanide or scandium, and a *p*-block main-group metal or a *d*-block transition metal. The rich structural chemistry of such compounds is discussed.

Keywords: Quaternary chalcogenides; Rare-earth compounds; Alkaline-earth compounds; Alkali compounds

1. Introduction

Although some binary rare-earth sulfides were prepared at the beginning of this century [1], research on binary and ternary rare-earth chalcogenides (S, Se, Te) accelerated in the late 1950s and 1960s [2,3] and continues to be an active area [4,5]. These materials adopt a wide range of structure types and display a variety of interesting physical properties [4]. Some have potential applications, for example as luminescent materials [6,7], magneto-optical materials [8], and infrared windows [9]. Because of the similarity in chemical composition of some of these systems to the high-temperature superconducting cuprates, efforts have also been made to synthesize sulfide analogues of the cuprates [10, 11].

The structural features of a quaternary system are often more varied than those in binary or ternary systems. However, if some of the metal atoms disorder, the resultant structures may be those of pseudo-binary or pseudo-ternary compounds [12–15]. We anticipated that cation disorder could be avoided through the use of elements with different coordination preferences [16]. This approach has been successful, and we describe here the syntheses and rich structural chemistry of new quaternary chalcogenides that contain three metal elements from different major blocks of the Periodic Table, namely an *s*-block alkali- or alkaline-earth metal, an *f*-block lanthanide or scandium, and a *p*-block main-group metal or a *d*-block transition metal.

2. Previously known compounds

Whereas many ternary chalcogenides that contain a rare-earth element and another metal are known, relatively few quaternary chalcogenides that contain a rare-earth element and two other metals are known. In particular, here we are concerned with compounds of the type A/Ln/M/Q, where A is an alkali- or alkaline-earth metal, Ln is a rare-earth metal or sometimes Sc, M is a main-group or transition metal, and Q is S or Se. No tellurides of this type are known.

Flahaut [4] has reviewed such compounds with two structure types: $CaLaAl_3S_7$ [17] and $La_2Sr_3Sn_3S_{12}$ (isostructural with $Eu_5Sn_3S_{12}$ (i.e. $Eu_3^{2+}Eu_2^{3+}Sn_3^{4+}S_{12}^{2-}$) [18]. More recently, Ibanez et al. [19] synthesized $NaNdGa_4S_8$, which crystallizes in a derivative of the $EuGa_2S_4$ structure type (consisting of GaS_4 tetrahedra and corner-sharing NdS_8 and NaS_8 square antiprisms;

* Corresponding author.

SSDI 0925-8388(95)01676-7

$NaLaGa_4S_8$ and $NaCeGa_4S_8$ also appear to crystallize in the same structure [6]. Carpenter and Hwu synthesized $CaYbInQ_4$ [20] and $Ca_4Ln_2In_4Q_{13}$ (Ln = Nd, Sm, Gd) [21]. The former crystallizes in the Mg_2SiO_4 structure type with edge-sharing YbQ_6-octahedral chains connected into layers by InQ_4 tetrahedra, and the latter contains edge-sharing CaQ_6 and InQ_6 octahedral chains, InQ_4 tetrahedra, and LnQ_8 bicapped-trigonal prisms. De la Mora and Goodenough prepared $Li_xMgYb_2Se_4$ by lithiation of $MgYb_2Se_4$ [22]. It maintains the spinel framework at low temperature but converts when annealed at high temperatures to a disordered NaCl structure.

3. Preparative methods

3.1. K/Ln/M/Q (M = Si, Ge, Sn, Q = S, Se) systems

These compounds were prepared by the high-temperature reactions of elemental Si, Ge, or Sn with the binary chalcogenides K_2Q_5 and Ln_2Q_3 [23, 24]. The products of most of these reactions are primarily crystals and powders of $KLnMQ_4$, mixed with small amount of impurities. For the K/Y/Sn/S system, small crystals of $K_2Y_4Sn_2S_{11}$ grew together with various binary and ternary sulfides.

3.2. Ba/Ln/M/Q (M = Cu, Ag) systems

Several compounds with the general formula $BaLnMQ_3$ [24–26] or $Ba_2LnM_5Q_6$ [27] were prepared by the high-temperature reactions of elemental Cu or Ag and Q with the binary chalcogenides BaQ and Ln_2Q_3. Whereas these reactions often afforded single crystals, an alternative synthetic route involving halide fluxes was used to grow some of the single crystals of $BaLaCuSe_3$, $BaCeCuSe_3$, $BaYCuSe_3$, $BaErCuSe_3$, $BaErAgSe_3$, and $BaYAgSe_3$. Halide fluxes have been used in the growth of chalcogenide crystals for over a century [28], and recently several new quaternary chalcogenides have been crystallized from such fluxes [20,21]. In the present work a halide flux was coupled with a high-temperature metathesis reaction between $BaBr_2$ and K_2Se_3 to circumvent the need to presynthesize BaSe and Ln_2Se_3. A similar approach was used [29] in the growth of $CdCr_2Se_4$ single crystals from a mixture of Cd, Se, and $CrCl_3$. We have used a starting mixture of $BaBr_2$, Ln, Cu or Ag, K_2Se_3, and KBr with a loading equivalent by weight to $BaLnMSe_3$:$BaBr_2$/KBr = 1:2.5. The flux had $BaBr_2$:KBr = 52:48, corresponding to the eutectic with a melting point of 609 °C [30].

4. Descriptions of the structures

4.1. $KLnMQ_4$ (Ln = La, Nd, Gd, Y; M = Si, Ge; Q = S, Se)

Eight members of this series have been synthesized [23]; from crystallographic unit-cell data they are isostructural. The structures $KLaGeS_4$ and $KLaGeSe_4$ (Fig. 1) were determined from single-crystal data. These structures have two-dimensional layers $^2_\infty[LnGeQ_4^-]$ separated by K^+ ions. Within a layer (Fig. 2) there are GeQ_4 tetrahedra whose Q–Ge–Q bond angles range from 101 to 115°. The Ge–S bond lengths range from 2.175(1) to 2.220(1) Å and the Ge–Se bond lengths range from 2.308(2) to 2.354(2) Å. Also within a layer are LaQ_7 monocapped trigonal prisms. The La–Q bond lengths range from 2.898(1) to 3.123(1) Å in $KLaGeS_4$ and from 3.023(2) to 3.210(2) Å in $KLaGeSe_4$. The LaQ_7 trigonal prisms (delineated by the thin solid lines in Fig. 2) share two of the three edges of their rectangular faces to form chains along the *b* direction, whereas the third edge is shared with a GeQ_4 tetrahedron. This tetrahedron in turn shares its other two vertices with two trigonal prisms in the adjacent chain. These chains are cross-linked not only by GeQ_4 tetrahedra, but also by Q atoms in the neighboring chain that cap one rectan-

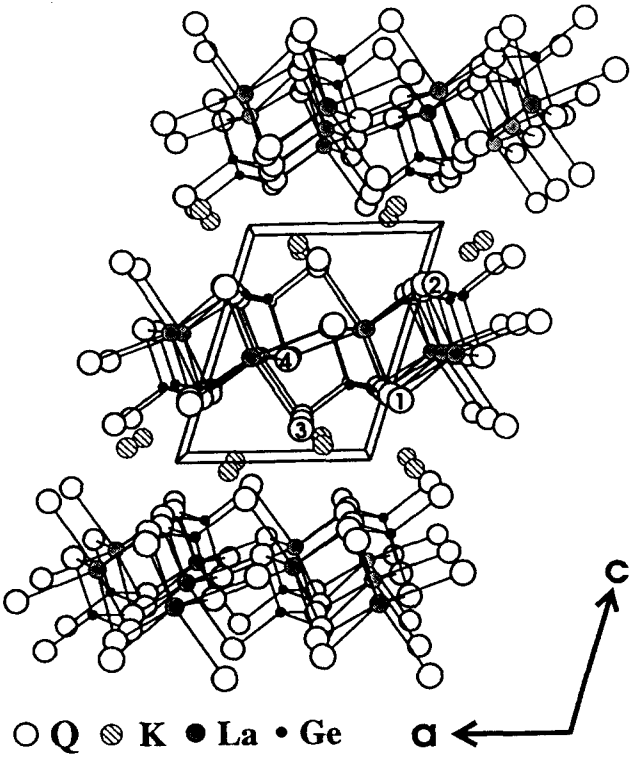

Fig. 1. View along the *b* axis of the $KLaGeQ_4$ structure.

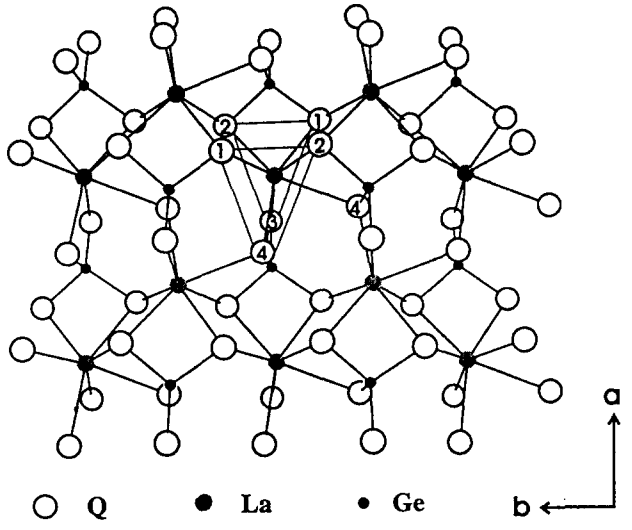

Fig. 2. View along the c^* axis of a $^2_\infty[LnGeQ_4^-]$ layer.

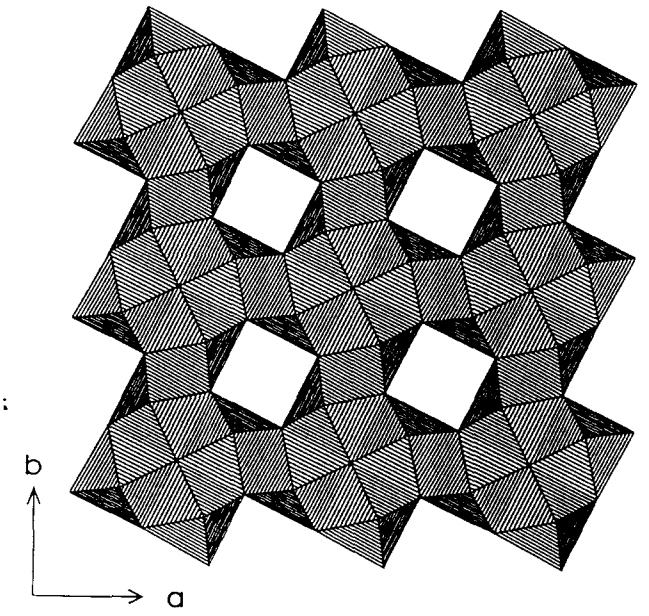

Fig. 4. A polyhedral representation of a layer of the Y–S octahedra in the $K_2Y_4Sn_2S_{11}$ structure.

gular face of each trigonal prism. As shown in Fig. 2, all caps point in the same direction along the b axis. The resultant structure of $KLaGeQ_4$ is non-centrosymmetric.

4.2. $K_2Y_4Sn_2S_{11}$

In this structure [24] (Fig. 3) there are YS_6 octahedra and SnS_4 tetrahedra. Through edge sharing the octahedra are connected into a layer along the a–b plane (Fig. 4). A pair of such layers forms a slab in the structure, and these slabs are cross-linked by Sn_2S_6 units. The slabs resemble the NaCl structure, with the two inner layers consisting of both cations and anions and two outer layers consisting only of anions. The S atoms in the inner layers are coordinated by only three Y atoms in the same layer and a fourth one in the adjacent layer, and hence one fifth of the cation sites are vacant (as shown in Fig. 4). The Sn_2S_6 units, which are pairs of edge-sharing SnS_4 tetrahedra, resemble the building unit of the SiS_2 structure type [31], and are also found as isolated $Sn_2S_6^{4-}$ anions in the structure of $Na_4Sn_2S_6 \cdot 14H_2O$ [32]. In the $K_2Y_4Sn_2S_{11}$ structure, the adjacent pairs of edge-sharing SnS_4 tetrahedra are oriented perpendicular to each other

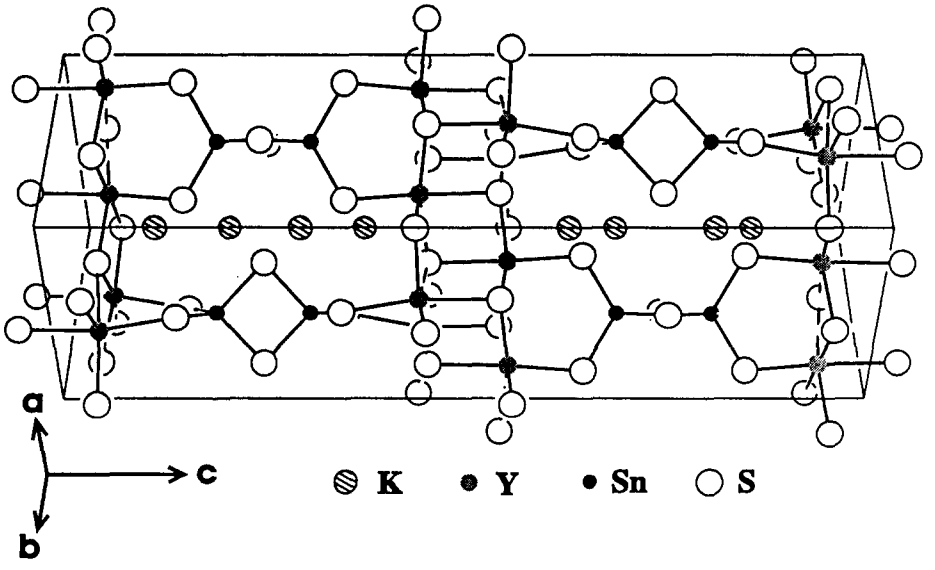

Fig. 3. View down [110] of the $K_2Y_4Sn_2S_{11}$ structure.

(Fig. 3), and the voids between the tetrahedral pairs are filled by K^+ cations, which can also be viewed as occupying the channels along the [110] and [1$\bar{1}$0] directions. Both the SnS_4 tetrahedra and the YS_6 octahedra are distorted, with the S–Sn–S bond angles ranging from 94.74(6) to 120.73(7)° and the *cis* S–Y–S angles ranging from 83.32(4) to 104.27(4)°. The Y–S bond lengths range from 2.679(1) to 2.792(2) Å and the Sn–S bond lengths range from 2.363(1) to 2.438(1) Å.

4.3. $BaErAgS_3$

The $BaErAgS_3$ structure [24] (Fig. 5) contains ErS_6 octahedra. The Er–S bond lengths range from 2.724(1) to 2.764(2) Å. Four of the shorter Ag–S bonds have lengths ranging from 2.543(1) to 2.748(1) Å. These values are close to the Ag–S bond lengths in the AgS_4 tetrahedra in $AgGaS_2$ (2.556(1) Å) [33]. However, the AgS_4 tetrahedron in the $BaErAgS_3$ structure is highly distorted, with S–Ag–S angles ranging from 92.30(4) to 129.64(1)°. The coordination environment of the Ag atom can be better described as trigonal bipyramidal, with a fifth S atom included in the coordination sphere at a distance of 3.167(1) Å. In this structure the ErS_6 octahedra share edges in a zigzagged manner and form a double chain along the *b* axis (Fig. 6). These chains of octahedra then share corners to form $^2_\infty[Er_2S_5^{4-}]$ layers that are connected through pairs of corner-sharing AgS_5 trigonal bipyramids (Ag_2S_9) units). The overall structure comprises a three-dimensional framework of ErS_6 octahedra and AgS_5 trigonal bipyramids with channels within that extend along the *b* axis. Ba^{2+} ions occupy the monocapped trigonal prismatic sites inside the channels.

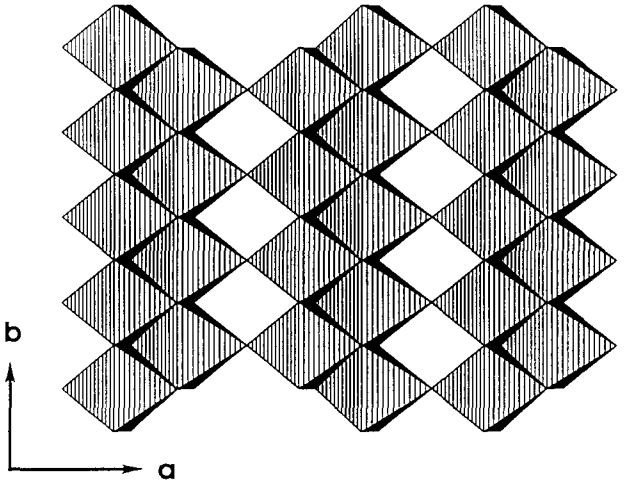

Fig. 6. View along the c^* axis of a polyhedral representation of an $^2_\infty[Er_2S_5^{4-}]$ octahedral layer in the $BaErAgS_3$ structure.

4.4. $BaErCuS_3$ and $BaYAgSe_3$

These materials [26] crystallize in the $KZrCuS_3$ [34] structure type illustrated in Fig. 7 for $BaYAgSe_3$. In these structures there are two-dimensional layers $^2_\infty[LnMQ_3^{2-}]$ (Ln = Er, Y; M = Cu, Ag; Q = S, Se) (Fig. 8) separated by Ba^{2+} ions. The layers contain LnQ_6 octahedra and MQ_4 tetrahedra that are close to regular, with the Q–M–Q bond angles ranging from 107.74(4) to 112.9(1)° and *cis* Q–Ln–Q angles ranging from 84.96(2) to 95.04(2)°. All *trans* Q–Ln–Q angles are fixed at 180° by symmetry. In $BaErCuS_3$ the Er–S bond lengths (2.677(1)–2.735(2) Å) are slightly shor-

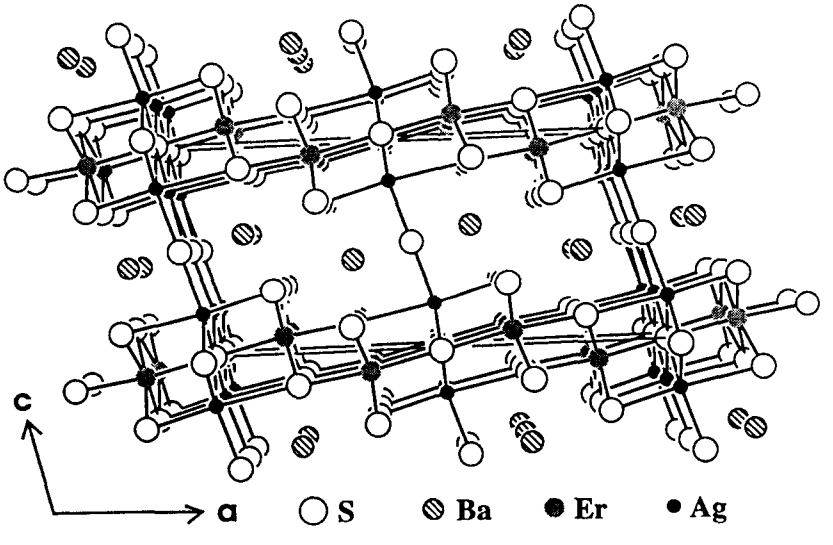

Fig. 5. View along the *b* axis of the $BaErAgS_3$ structure.

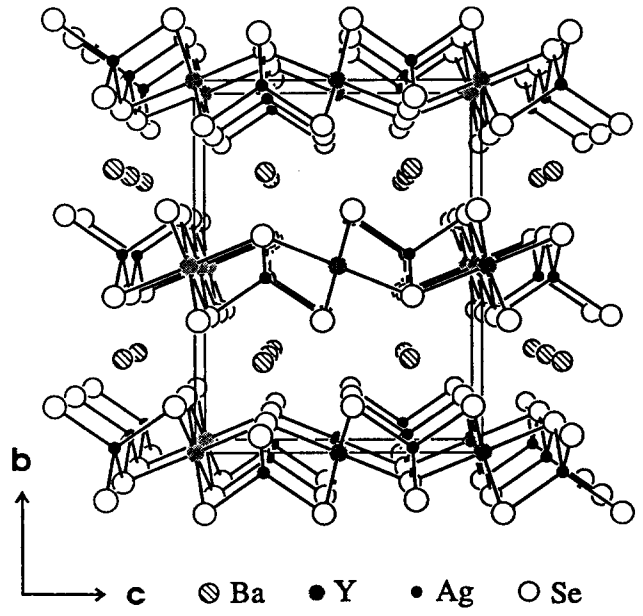

Fig. 7. View along the *a* axis of the $BaYAgSe_3$ structure.

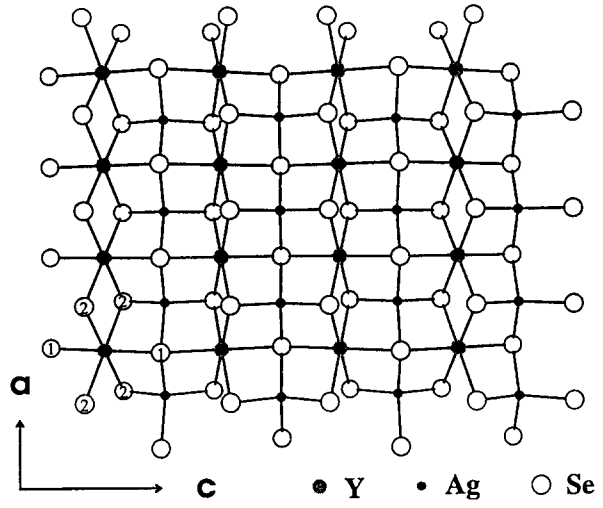

Fig. 8. View along the *b* axis of a $^{2}_{\infty}[YAgSe_3^{2-}]$ layer.

ter than those in $BaErAgS_3$ (2.724(1)–2.764(2) Å), and the Cu–S bond lengths (2.339(2)–2.392(2) Å) are similar to those in $BaLaCuS_3$ (2.338(1)–2.398(1) Å). The bond lengths in $BaYAgSe_3$ (Y–Se: 2.879(1)–2.910(1) Å; Ag–Se: 2.600(1)–2.624(1) Å) also compare well with those in the literature, e.g. Y–Se in YSeF [35] (2.81(1)–2.94(1) Å) and Ag–Se in β'-Ag_8GeSe_6 [36] (2.62(1)–2.94(1) Å). In the present structures the LnQ_6 octahedra share an opposite pair of edges and form chains along the *b* direction. The MQ_4 tetrahedra form corner-sharing chains along the *b* direction. The LnQ_6 chains in turn are cross-linked through sharing two of the corners of each octahedron and by sharing edges with MQ_4 tetrahedra in between the octahedral chains.

4.5. $BaLaCuS_3$

The $BaLaCuS_3$ structure [25] consists of a three-dimensional framework of LaS_7 monocapped trigonal prisms and CuS_4 tetrahedra (Fig. 9). It also exhibits one-dimensional character in the form of channels that extend along the *b* axis. Ba^{2+} ions are accommodated in these channels. The La–S bond lengths (2.915(1)–3.028(1) Å) are similar to those in $KLaGeS_4$ (2.898(1)–3.123(1) Å) and the Cu–S bond lengths (2.338(1)–2.398(1) Å) are similar to those in $BaErCuS_3$ (2.339(2)–2.392(2) Å). The CuS_4 tetrahedron is significantly distorted (S–Cu–S bond angles: 103.08(4)–126.53(5)°).

4.6. $BaLaCuSe_3$

As prepared, $BaLaCuSe_3$ crystallizes in a layered structure (Fig. 10) in the space group *Pnma* (β), but powder diffraction patterns of ground polycrystalline samples reveal the presence of both the β phase and the α phase, which is isostructural with $BaLaCuS_3$ (Fig. 9) [25]. A comparison of Figs. 7 and 10 shows the *Pnma* structure of β-$BaLaCuSe_3$ to be very similar to the *Cmcm* structure adopted by $BaErCuS_3$ and $BaYAgSe_3$. The structures have the same atomic connectivity, but in the β-$BaLaCuSe_3$ structure all three pairs of *trans* Q–Ln–Q bonds of an $LaSe_6$ octahedron are bent slightly (174.43(3)–177.10(3)°), whereas they are linear in the $BaErCuS_3$ structure type. The La–Se bond lengths in β-$BaLaCuSe_3$ (2.940(2)–3.019(2) Å) are slightly shorter than those in $KLaGeSe_4$ (3.023(2)–3.210(2) Å), where La is seven-coordinated. The $CuSe_4$ tetrahedron is only

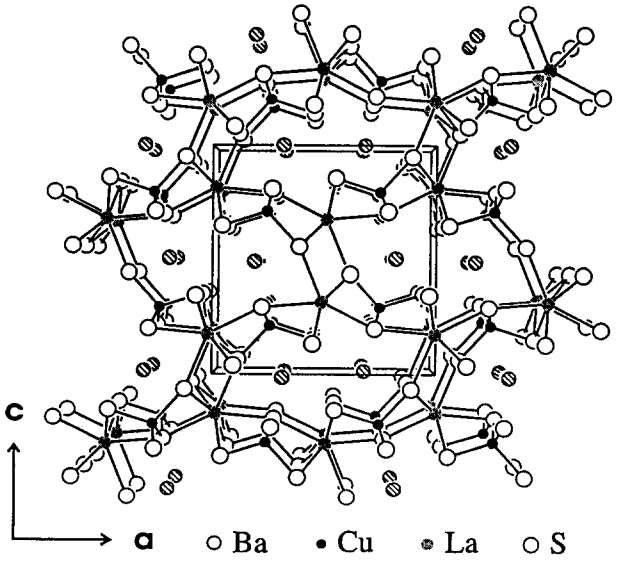

Fig. 9. View along the *b* axis of the $BaLaCuS_3$ structure.

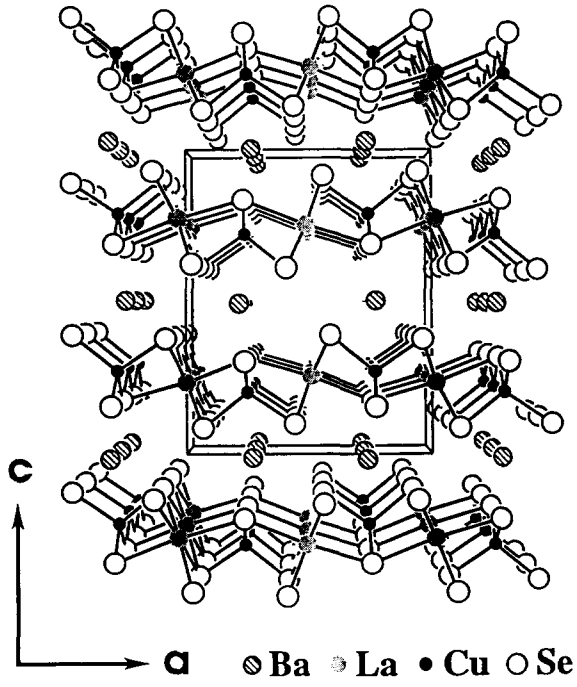

Fig. 10. View along the b axis of the β-$BaLaCuSe_3$ structure.

slightly distorted (Se–Cu–Se angles: 106.55(7)–112.83(7)°) and the Cu–Se bond lengths (2.478(2)–2.577(2) Å) are slightly longer than those in $K_2CuTaSe_4$ (2.456(2) Å) [37].

4.7. $Ba_2LaAg_5S_6$

The compound $Ba_2LaAg_5S_6$ [27] (Fig. 11) provides another example of a structure type with channels in a three-dimensional framework of metal–chalcogen coordination polyhedra, as seen in α-$BaLaCuQ_3$.

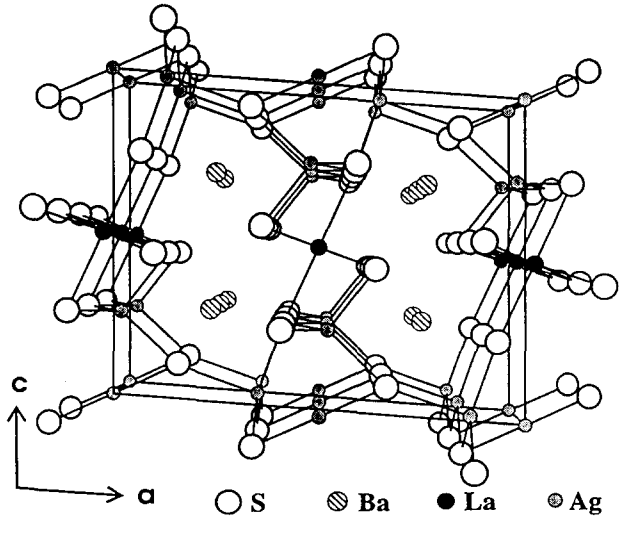

Fig. 11. View along b axis of the $Ba_2LaAg_5S_6$ structure.

Again, these channels accommodate Ba^{2+} ions. There are LaS_6 octahedra whose La–S bond lengths (2.892(3)–2.905(2) Å) are slightly shorter than those in the LaS_7 polyhedron in $KLaGeS_4$ (2.898(1)–3.123(1) Å). In most chalcogenides the coordination number of La is 7–9; coordination number 6, as in $Ba_2LaAg_5S_6$ and β-$BaLaCuSe_3$, is uncommon. The only other examples known to us are LaS [38] and LaSe [39], both of which adopt the NaCl structure. In $Ba_2LaAg_5S_6$ there are three crystallographically distinct Ag atoms. Two of these form AgS_4 tetrahedra with normal Ag–S bond lengths (2.563(3)–2.854(3) Å). The third forms a linear AgS_2 unit with an Ag–S distance of 2.376(3) Å. Alternatively, one can discern a highly compressed octahedron around atom Ag(3), consisting of these two S atoms and the four next-nearest S atoms at 3.841(3) Å, too far away for bonding. Linear coordination of Ag is also found in Na_3AgS_2, where there are AgS_2^{3-} anions separated by Na^+ cations (Ag–S = 2.370(3) Å) [40].

5. Structural relationships

All of the compounds discussed in the last section are ordered and have crystallographically distinct sites for the three different types of metal atoms. In these compounds there are no Q–Q interactions, so formal oxidation states can be readily assigned as K(I), Ba(II), Ln(III), M(I) (M = Cu, Ag), M′(IV) (M′ = Si, Ge, Sn), and Q(−II). The cation ordering in these compounds is in contrast with systems that contain one of the smaller rare-earth elements and a small s-block metal. Thus cation disorder occurs in $CaYbInS_4$ [20] and in $CaYAgS_3$ and $CaYAgSe_3$, whose face-centered cubic structures are similar to that of $Li_xMgYb_2Se_4$.

The Ba/Ln/M/Q (M = Cu or Ag) systems adopt a variety of quaternary structure types. Within these systems more than 20 compounds have been synthesized [24–27], and their structural types are summarized in Fig. 12. The $BaErCuS_3$ structure type prevails among the compounds of the smaller rare-earth elements (Y, Er). This is understandable because these elements tend to prefer octahedral coordination. In the compounds that contain a larger rare-earth element (Nd, Ce) as well as Cu, the β-$BaLaCuSe_3$ structure type is adopted, which may be viewed as a distorted version [26] of the $BaErCuS_3$ structure type where chalcogen atoms are shifted so that *trans* Q–Ln–Q bond angles deviate from 180°. Only with La, the largest rare-earth element, in α-$BaLaCuSe_3$ and $BaLaCuS_3$ does a further distortion occur, leading to collapse of the layers. Comparing Figs. 9 and 10, one can see that the channel structure of the α-$BaLaCuQ_3$ phase can also be viewed as a stack of distorted layers

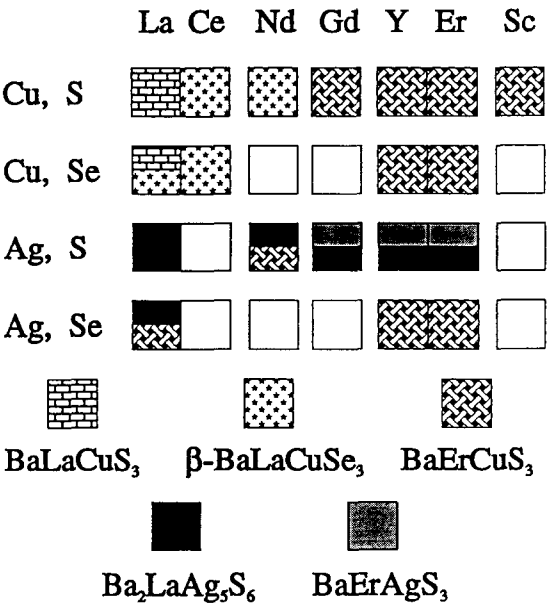

Fig. 12. Structure types in some of the Ba/Ln/M/Q (M = Cu, Ag) systems. Systems not investigated are left blank.

with some La–S bonds across the gaps. For $BaLaCuSe_3$, which has both phases, this literally corresponds to a structural transformation. Fig. 13 shows the local coordination environment of La in (a) β-$BaLaCuSe_3$ and (b) α-$BaLaCuS_3$. The transition from β to α corresponds to a distortion of an LaQ_6 octahedron in which the nearly linear diagonal Q–La–Q moiety is bent so as to open up the space necessary for the formation of an additional La–Q bond with a chalcogen atom from an adjacent layer. This results in monocapped trigonal prismatic geometry about La, as indicated by the thin solid lines. The α phase has a higher density ($6.04\ g\ cm^{-3}$ for α-$BaLaCuSe_3$ versus $5.81\ g\ cm^{-3}$ for β-$BaLaCuSe_3$), so that higher pressure should favor the former. In fact, for $BaLaCuSe_3$, the transition from the β phase to the α phase can be induced by mechanical grinding. Fig. 14 shows a set of X-ray powder diffraction patterns for $BaLaCuSe_3$. Curves (a) and (e) are the calculated patterns for the β and α phases respectively. Curve (b) is from a sample annealed at 600 °C for 2 days. This sample was gently crushed, but not ground, before the diffraction pattern was recorded. The β phase predominates. The same sample was then ground manually with an agate mortar and pestle for 5 min. The diffraction pattern (c) now shows the presence of both α and β phases. Grinding of the sample for a total of 30 min increases the proportion of the α phase (curve (d)). Only α-$BaLaCuSe_3$ is observed when the sample is ground for 2 h with a ball mill with acetone as the mineralizer. The α-$BaLaCuSe_3$ phase can be transformed to the β phase by annealing at elevated temperatures [25].

In the silver systems, whereas some compounds have the $BaEuCuS_3$ structure, others adopt two different structure types (Fig. 12) in which Ag has two- or five-coordination ($Ba_2LaAg_5S_6$ and $BaErAgS_3$). Because Cu normally adopts tetrahedral coordination in chalcogenides [41], it is not surprising that no Cu compounds exhibit either of these structure types.

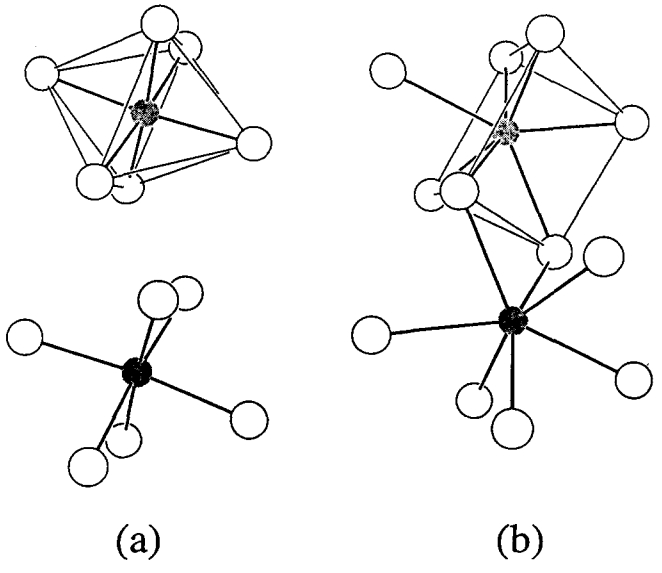

Fig. 13. Coordination geometry around La in (a) β-$BaLaCuSe_3$ and (b) α-$BaLaCuS_3$.

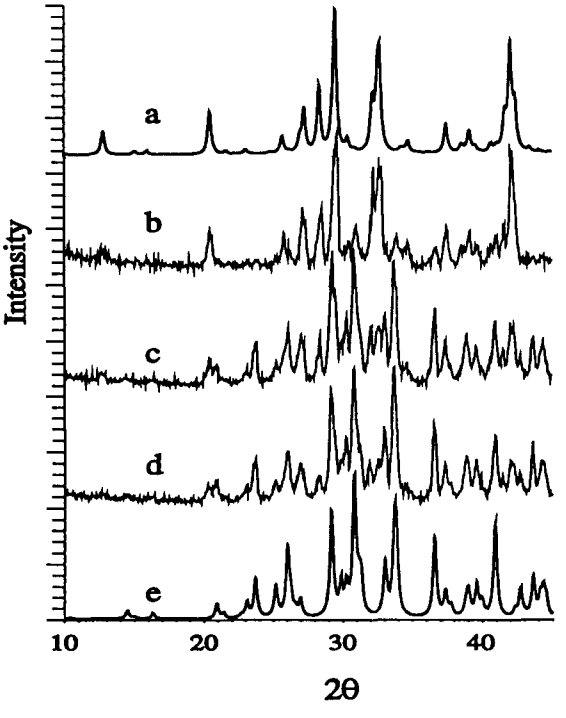

Fig. 14. Calculated and measured X-ray diffraction powder patterns (Cu Kα) of $BaLaCuSe_3$: (a) calculated for the β phase; (b) measured on an annealed sample; (c) measured on the sample after grinding for 5 min; (d) measured on the sample after grinding for 30 min; (e) calculated for the α phase.

In both the $BaErCuS_3$ and β-$BaLaCuSe_3$ structure types, there are edge-sharing octahedral chains that are connected by corner sharing. If these chains are further separated and connected only through the tetrahedra, they resemble the layers in the $CaYbInQ_4$ structure [20]. On the other hand, if these chains are paired up through edge-sharing, they resemble the layers in $K_2Y_4Sn_2S_{11}$ (Fig. 4 shows half of a double octahedral layer with vacant sites) or $BaErAgS_3$ (Fig. 6). The double chains of edge-sharing LnS_6 octahedra form layers through further edge-sharing, as in $K_2Y_4Sn_2S_{11}$, or through corner sharing, as in $BaErAgS_3$. In both structures the layers are separated by cations and the connection is made through a pair of coordination polyhedra around the third metal element.

The quaternary structure types are often closely related to ternary structure types. For example, the $NdYbS_3$ structure [42] comprises YbS_6-octahedral layers separated by eight-coordinated Nd^{3+} ions. Substitution of Ba^{2+} for Nd^{3+} and insertion of Cu^+ into a tetrahedral site leads to the $BaErCuS_3$ structure. The same kind of Er-chalcogen octahedral layers as in $BaErAgS_3$ are found in $BaSmS_2$ [43] and $ErAgSe_2$ [44] where such layers are connected through corner-sharing and form three-dimensional structures. Fig. 15 shows the structure of $ErAgSe_2$. The addition of the third metal atom into the structure effectively separates the layers and results in a structure framework that is only linked through Ag_2S_9 units in $BaErAgS_3$.

Two of the structure types discussed here are related to ternary europium sulfides. The $KLaGeS_4$ structure type is related to that of Eu_2GeS_4 [45] The latter (Fig. 16) has two Eu^{2+} sites, both of which are seven coordinated, and the structure extends in all three dimensions. The substitution of Ln^{3+} for Eu(1) and K^+ for Eu(2) results in the $KLaGeQ_4$ structure type. Although the framework of the two structure types is similar, as a result of the very electropositive nature of K^+ the $KLaGeQ_4$ structure comprises alternating $^2_\infty[LnMQ_4^-]$ layers and K^+ layers. K^+, which is larger than Eu^{2+}, is eight coordinated and the $KLaGeQ_4$ structure type is distorted slightly from that of Eu_2GeS_4. β-$BaLaCuSe_3$ is isostructural with Eu_2CuS_3 (i.e. $Eu^{2+}Eu^{3+}Cu^+S_3^{2-}$) [46], with La^{3+} ions occupying the same octahedral sites as the Eu^{3+} ions and the Ba^{2+} ions occupying the same seven-coordinate sites as the Eu^{2+} ions.

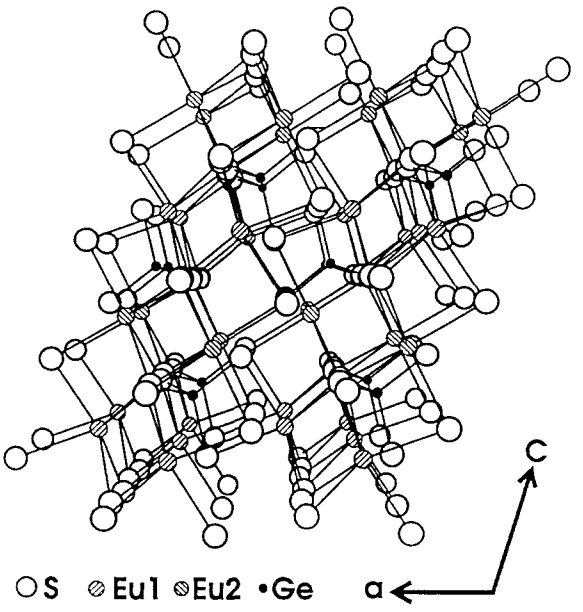

Fig. 16. View of the Eu_2GeS_4 structure along the b axis.

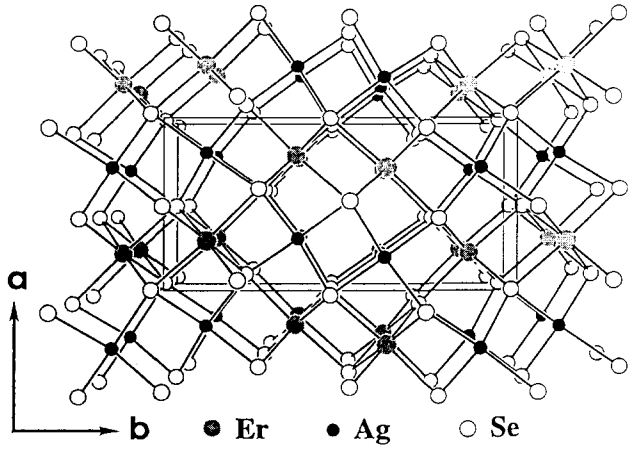

Fig. 15. View along the c axis of the $ErAgSe_2$ structure.

6. Physical properties

Consistent with their stoichiometric nature and the absence of Q–Q bonds, all of these compounds are poor conductors. Magnetic susceptibility measurements show that $KNdGeS_4$, $KGdGeS_4$, $BaNdCuS_3$, and $BaGdCuS_3$ follow the Curie–Weiss law from 6 to 300 K, whereas $BaCeCuS_3$ and $BaCeCuSe_3$ display, in addition, temperature-independent paramagnetism [23,26]. Their effective Bohr magneton numbers at room temperature are consistent with the theoretical values for the corresponding Ln^{3+} ions [47].

Because crystals large enough for optical transmission measurements were not available, diffuse reflective UV-visible spectra were recorded on single-phase polycrystalline samples. The reflectivity of some of the compounds shows a sharp decrease, which corresponds to the absorption edge: hence the optical band-gap values (Table 1) were deduced from the spectra [23,25,26]. Examples of the spectra for $BaNdCuS_3$ and $BaNdAgS_3$ are shown in Fig. 17. A steep region is not

Table 1
Measured optical band gaps of several $BaLnMQ_3$ compounds

Compound	Band Gap (eV)
$BaYCuS_3$	2.61(3)
$BaGdCuS_3$	2.41(3)
$BaNdCuS_3$	2.39(3)
$BaLaCuS_3$	2.00(2)
$BaNdAgS_3$	2.31(4)

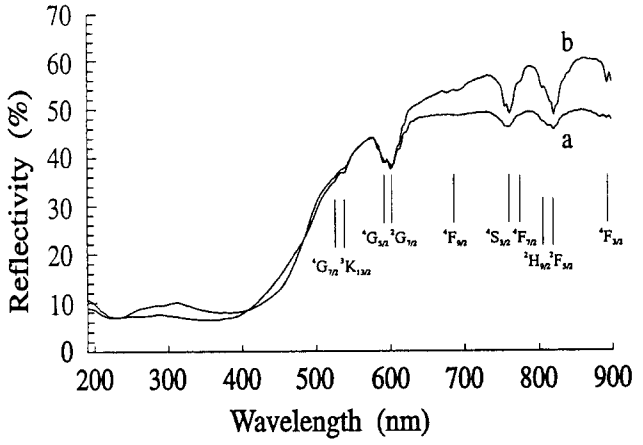

Fig. 17. Diffuse reflective UV-visible spectra of (a) $BaNdCuS_3$ and (b) $BaNdAgS_3$.

found in the spectra of several compounds, including $BaLaCuSe_3$, $BaCeCuS_3$, and $BaCeCuSe_3$, so a band-gap value cannot be obtained from the optical data. There is structure in the high-energy end of all these spectra. When the spectra of analogues between sulfide and selenide are compared, the spectrum of the selenide is similar to that of the sulfide but is shifted towards lower energy. This shift may be the result of the generally higher bonding energy and ionicity in sulfides compared with selenides. In the spectra of $BaNdMS_3$ (M = Cu, Ag), there are several absorption peaks at energies lower than the band gap that result from transitions associated with 4f electronic states.

7. Concluding remarks

The synthesis of new compounds is the necessary beginning for the establishment of relationships among stoichiometry, structure, and physical properties of solid-state compounds. The newly synthesized members of the A/Ln/M/Q quaternary systems described here show a wide range of structural features that can be described by the packing of metal–chalcogen polyhedra. Much more needs to be done. Thus the further characterization of the optical properties of these materials, preferably on single crystals, combined with theoretical calculations, will help elucidate their intrinsic bonding characteristics. But note that the systems described here involve only a very limited range of the element M; myriad systems, presumably possessing new structural features, remain unexplored. As the concentrated effort on the cuprates has revealed, an understanding of structural relationships is possible in very complex systems involving more than three types of metal atom. Unfortunately, despite massive and heroic efforts, especially for the cuprates, the understanding of physical properties and their relation to structure may be charitably described as primitive. But if a compound has not been synthesized its physical properties cannot be measured and ultimately understood, and that simple truism remains a major impetus for the synthesis of new solid-state materials.

Acknowledgments

The research described here was supported by the US National Science Foundation (Grant DMR91-14934). Use was made of Central Facilities supported by the US National Science Foundation through the Northwestern University Materials Research Center (Grant DMR91-20521).

References

[1] W. Biltz, *Z. Anorg. Chem.*, *71* (1911) 427–438.
[2] J. Flahaut and P. Laruelle, in L. Eyring (ed.), *Progress in the Science and Technology of the Rare Earths*, Vol. 3, Pergamon Press, Oxford, 1968, pp. 149–208.
[3] J. Flahaut, in L. Eyring (ed.), *Progress in the Science and Technology of the Rare Earths*, Vol. 3, Pergamon Press, Oxford, 1968, pp. 209–283.
[4] J. Flahaut, in K.A. Gschneidner Jr. and L.R. Eyring (eds.), *Handbook on the Physics and Chemistry of Rare Earths*, Vol. 4, North-Holland Publishing Company, Amsterdam, New York, Oxford, 1979, pp. 1–88.
[5] A.A. Eliseev, O.A. Sadovskaya and G.M. Kuz'micheva, *Inorg. Mater. Engl. Transl.*, *18* (1982) 1435–1450.
[6] T.E. Peters and J.A. Baglio, *J. Electrochem. Soc.*, *119* (1972) 230–236.
[7] R. Ibañez, A. Garcia, C. Fouassier and P. Hagenmuller, *J. Solid State Chem.*, *53* (1984) 406–414.
[8] B.A. Kolesov and I.G. Vasilyeva, *Mater. Res. Bull.*, *27* (1992) 775–781.
[9] J.A. Savage and K.L. Lewis, *Proc. SPIE Int. Soc. Opt. Eng*, *683 (Infrared and Optical Transmitting Materials)* (1986) 79–84.
[10] R. Ithnin, D.J. Gilbert, S. Arnold and J.V. Acrivos, *NATO ASI Ser., Ser. B, 172 (Chem. Phys. Intercalation)* (1987) 507–509.
[11] M.P. Kulakov, S.A. Zver'kov, V.K. Gartman, N.N. Kolesnikov, O.V. Zharikov and G.I. Peresada, *Inorg. Mater. Engl. Transl.*, *27* (1992) 1653–1656.
[12] Y.-J. Lu and J.A. Ibers, *J. Solid State Chem.*, *94* (1991) 381–385.
[13] T.D. Brennan and J.A. Ibers, *J. Solid State Chem.*, *97* (1992) 377–382.
[14] P. Wu, Y.-J. Lu and J.A. Ibers, *J. Solid State Chem.*, *97* (1992) 383–390.

[15] P. Wu and J.A. Ibers, *Acta Crystallogr., Sect. C: Cryst. Struct. Commun., 49* (1993) 126–129.
[16] S.A. Sunshine, D.A. Keszler and J.A. Ibers, *Acc. Chem. Res., 20* (1987) 395–400.
[17] A.-M. Lozac'h, M. Guittard and J. Flahaut, *C.R. Séances Acad. Sci., Ser. C, 275* (1972) 809–812.
[18] S. Jaulmes and M. Julien-Pouzol, *Acta Crystallogr., Sect. B: Struct. Crystallogr. Cryst. Chem., 33* (1977) 1191–1193.
[19] R. Ibanez, P. Gravereau, A. Garcia and C. Fouassier, *J. Solid State Chem., 73* (1988) 252–258.
[20] J.D. Carpenter and S.-J. Hwu, *Chem. Mater., 4* (1992) 1368–1372.
[21] S.-J. Hwu and J.D. Carpenter, Abstr. Pap.-Am. Chem. Soc., *204th National Meeting*, Washington, D.C. (1992) INOR 393.
[22] P. de la Mora and J.B. Goodenough, *J. Solid State Chem., 70* (1987) 121–128.
[23] P. Wu and J.A. Ibers, *J. Solid State Chem., 107* (1993) 347–355.
[24] P. Wu and J.A. Ibers, *J. Solid State Chem., 110* (1994) 156–161.
[25] A.E. Christuk, P. Wu and J.A. Ibers, *J. Solid State Chem., 110* (1994) 330–336.
[26] P. Wu, A.E. Christuk and J.A. Ibers, *J. Solid State Chem., 110* (1994) 337–344.
[27] P. Wu and J.A. Ibers, *Z. Kristallogr., 208* (1993) 35–41.
[28] D. Elwell and H.J. Scheel, *Crystal Growth from High-Temperature Solutions*, Academic Press, London, 1975.
[29] A.W. Sleight, *Inorg. Synth., 14* (1974) 155–157.
[30] R.S. Roth, T. Negas and L.P. Cook, *Phase Diagrams for Ceramists*, Vol. V, American Ceramic Society, Columbus, 1983, p. 5, Fig. 5600.
[31] J. Peters and B. Krebs, *Acta Crystallogr., Sect. B: Struct. Crystallogr. Cryst. Chem., 38* (1982) 1270–1272.
[32] B. Krebs, S. Pohl and W. Schiwy, *Z. Anorg. Allg. Chem., 393* (1972) 241–252.
[33] S.C. Abrahams and J.L. Bernstein, *J. Chem. Phys., 59* (1973) 1625–1629.
[34] M.F. Mansuetto, P.M. Keane and J.A. Ibers, *J. Solid State Chem., 101* (1992) 257–264.
[35] Nguyen-Huy-Dung and P. Laruelle, *Acta Crystallogr., Sect. B: Struct. Crystallogr. Cryst. Chem., 33* (1977) 3360–3363.
[36] D. Carré, R. Ollitrault-Fichet and J. Flahaut, *Acta Crystallogr., Sect. B: Struct. Crystallogr. Cryst. Chem., 36* (1980) 245–249.
[37] Y.-J. Lu, P. Wu and ' A. Ibers, *Eur. J. Solid State Inorg. Chem., 30* (1993) 101–110.
[38] A. Iandelli, *Gazz. Chim. Ital., 85* (1955) 881–887.
[39] M. Guittard and A. Benacerraf, *C.R. Hebd. Séances Acad. Sci., 248* (1959) 2589–2591.
[40] K.O. Klepp and W. Bronger, *J. Less-Common Met., 106* (1985) 95–101.
[41] P.M. Keane, Y.-J. Lu and J.A. Ibers, *Acc. Chem. Res., 24* (1991) 223–229.
[42] D. Carré and P. Laruelle, *Acta Crystallogr., Sect. B: Struct. Crystallogr. Cryst. Chem., 30* (1974) 952–954.
[43] J.D. Carpenter and S.-J. Hwu, *Acta Crystallogr., Sect. C: Cryst. Struct. Commun., 48* (1992) 1164–1167.
[44] M. Julien-Pouzol and P. Laruelle, *Acta Crystallogr., Sect. B: Struct. Crystallogr. Cryst. Chem., 33* (1977) 1510–1512.
[45] G. Bugli, J. Dugué and S. Barnier, *Acta Crystallogr., Sect. B: Struct. Crystallogr. Cryst. Chem., 35* (1979) 2690–2692.
[46] P. Lemoine, D. Carré and M. Guittard, *Acta Crystallogr., Sect. C: Cryst. Struct. Commun., 42* (1986) 390–391.
[47] J.H. Van Vleck, *The Theory of Electric and Magnetic Susceptibilities*, Oxford University Press, London, 1932.